Laser wakefield acceleration by petawatt ultrashort laser pulses

L. M. Gorbunov
P. N. Lebedev Physics Institute, Russian Academy of Sciences, Leninskii prospect 53, Moscow 119991, Russia

S. Yu. Kalmykov[a)]
The Department of Physics and Institute for Fusion Studies, The University of Texas at Austin, One University Station C1500, Austin, Texas 78712 and Centre de Physique Théorique (UMR 7644 du CNRS), École Polytechnique, 91128 Palaiseau, France

P. Mora
Centre de Physique Théorique (UMR 7644 du CNRS), École Polytechnique, 91128 Palaiseau, France

(Received 1 October 2004; accepted 6 December 2004; published online 3 February 2005)

An ultrashort (about 30 fs) petawatt laser pulse focused with a wide focal spot (about 100 μm) in a rarefied plasma ($n_0 \sim 10^{17}$ cm^{-3}) excites a nonlinear plasma wakefield which can accelerate injected electrons up to GeV energies without any pulse channeling. Under these conditions, propagation of the laser pulse with an overcritical power for relativistic self-focusing is almost the same as in vacuum. The nonlinear quasiplane plasma wave, whose amplitude and phase velocity vary along the laser path, effectively traps and accelerates injected electrons with a wide range of initial energies. Electrons accelerated over two Rayleigh lengths (about 8 cm) can gain energies up to 1 Gev. In particular, the electrons trapped from a long ($\tau_b \sim 330$ fs) nonresonant electron beamlet of 1 MeV particles eventually form a low emittance bunch with energies in the range 900 ± 50 MeV. These conclusions follow from two-dimensional simulations performed in cylindrical geometry by means of the fully relativistic time-averaged particle code WAKE [P. Mora and T. M. Antonsen, Jr., Phys. Rev. E **53**, R2068 (1996); Phys. Plasmas **4**, 217 (1997)]. © *2005 American Institute of Physics*. [DOI: 10.1063/1.1852469]

I. INTRODUCTION

In the original, or "standard," scheme of laser wakefield acceleration[1,2] (LWFA), a laser pulse of duration smaller than a period of plasma oscillation, $\tau_p = 2\pi/\omega_p$, excites an electron plasma wave (wakefield) with a phase velocity close to the speed of light [here and elsewhere, $\omega_p = (4\pi n_0 e^2/m)^{1/2}$ is the electron plasma frequency, n_0 is the electron plasma density, m and $-|e|$ are the electron mass at rest and charge]. When the electron density perturbation exceeds the background density, the accelerating electric field of the nonlinear wake can reach tens of GV/m, which is three orders of magnitude higher than that which can be achieved in the conventional accelerators without material breakdown. To excite such a wakefield, a short laser pulse of very high intensity is needed, that is, $I_0 \lambda_0^2 > 1.4 \times 10^{18}$ W cm^{-2} μm^2 (where λ_0 is a laser wavelength). In previous experiments,[3] in which the laser energy was lower, reaching this range of intensities required tight focusing of the beam. The laser focal spot of radius $r_0 \sim 10$ μm gave an acceleration length on the order of a few millimeters (estimated as the Rayleigh length doubled, $2Z_R = 2\pi r_0^2/\lambda_0$). The observed energy gain of electrons injected in the wake was thus moderate in spite of a high accelerating gradient. Also, the plasma wake driven by a tightly focused laser is very narrow, and thus is ineffective for trapping and accelerating injected electrons: the scale of radial variation was considerably smaller than the axial wavelength, and most of the electrons were expelled by strong radial electric fields. Only few electrons were trapped and accelerated in the three-dimensional potential wells.[3]

The chirped-pulse amplification laser systems of the new, petawatt ($P \sim 10^{15}$ W) generation[4] are capable of producing ultrashort pulses (tens of femtoseconds) which can be focused with a relatively large focal spot, $r_0 \sim 100$ μm, yet have a relativistic intensity ($I_0 > 10^{18}$ W/cm^2) on axis. In this case, the effective acceleration distance (two Rayleigh lengths) is naturally elongated to about 10 cm, and the GeV energy range can be achieved by using the standard LWFA technique without external optical guiding.[2] In the scheme proposed, the plasma wavelength is smaller than the wake radial size. The large transverse extent of the wakefield structure reduces the adverse effect of radial forces on accelerated electrons.

Anticipating this attractive chance to reach the GeV range of electron energy using the standard LWFA, we analyze in this paper, both theoretically and numerically, the details of laser pulse and wakefield evolution, and simulate the acceleration of an electron bunch in a wide range of parameters typical of those prospective experiments. The simulations have been carried out using the code WAKE.[5,6] The laser parameters in the simulations are fixed: the laser wavelength $\lambda_0 = 0.8$ μm, the pulse energy 30 J, the pulse duration $\tau_L = 30$ fs, the radius of focal spot $r_0 = 100$ μm (hence, the maximum intensity in vacuum is $I_0 \approx 6.4 \times 10^{18}$ W/cm^2). In the simulations of electron acceleration, the electron density of the unperturbed plasma is $n_0 = 1.12 \times 10^{17}$ cm^3, which gives a period of plasma oscillation of $\tau_p \approx 330$ fs and a

[a)]Electronic mail: kalmykov@physics.utexas.edu

plasma wavelength of $\lambda_p = 2\pi/k_p \approx 100\ \mu$m (where $k_p = \omega_p/c$). The normalized pulse duration and width are then $\omega_p \tau_L = 0.56$ and $k_p r_0 = 6.28$, respectively. The relativistic factor corresponding to the laser group velocity is $\gamma_g \equiv \omega_0/\omega_p = 125$. The laser power thus exceeds by a factor of 4 the critical power for relativistic self-focusing, $P_{\rm cr} = 16.2(\omega_0/\omega_p)^2$ GW.[7]

This paper is organized as follows. A numerical study of the nonlinear effects in propagation of an ultrashort, petawatt laser pulse through rarefied plasma is given in Sec. II. The simulations, supported by the analytical treatment, show that for the parameters chosen, mutual cancellation of the relativistic and ponderomotive nonlinearities of the laser pulse occurs. It is only for very high intensities and/or electron densities (such that the critical power $P_{\rm cr}$ is exceeded by more than a factor of 4) that the nonlinearity produces some effect on the pulse shape.

Section III addresses the effect of laser pulse transverse evolution from propagation through the focus on the phase velocity of the two-dimensional (2D) nonlinear wakefield. The effect originates from the relativistic nonlinearity of the plasma wake. The amplitude of the wakefield is proportional to the laser intensity which grows (drops) as the pulse focuses (diverges). The relativistic reduction in frequency is in turn proportional, in the weakly relativistic approximation, to the wake amplitude squared. Therefore, as the pulse approaches the focal plane, the wake period stretches and its phase velocity drops below the pulse group velocity $v_g = c^2 k_0/\omega_0$. Beyond the focal plane the wake period shrinks and tends to the linear limit τ_p at infinity. At this stage, the wake phase accelerates and can become superluminous (i.e., exceeds not only the pulse group velocity in plasma but also the vacuum speed of light). A similar effect was discussed previously for the case of longitudinally inhomogeneous plasmas.[8] While the laser focuses, the growth of the wake amplitude combined with the reduction in phase velocity provides the conditions for highly efficient trapping of nonresonant injected electrons, $\gamma_{e0} \ll \gamma_g$ [here and below, $\gamma_{e0} \equiv (1 - v_{e0}^2/c^2)^{-1/2}$ is the initial Lorentz factor of the injected electrons corresponding to the velocity v_{e0} at the point of injection].

Details of the acceleration of resonant electron bunches by the wakefield are considered in Sec. IV. Numerical simulations show that a low energy spread of accelerated electrons can be achieved under resonant conditions $\gamma_{e0} \approx \gamma_g$ or $\gamma_{e0} \approx \gamma_{p0}$ (where γ_{p0} is a relativistic factor given by the local phase velocity of the wake plasma wave at the point of electron injection) only for ultrashort electron bunches loaded directly in the accelerating and focusing quarter of the wake period ($\tau_p/4 \approx 80$ fs for the parameters given). Injection of an electron bunch longer than a quarter period results in spreading of the output energy spectrum since electrons trapped at different phases of the wake will be accelerated differently (the minimum energy gain corresponds to the injection at the bottom of the wake potential well). Injection of monoenergetic electron bunches with $\gamma_{e0} = \gamma_g = 125$ or $\gamma_{e0} = 42$ in the second period of wakefield gives similar results: after two Rayleigh lengths ($\sim$8 cm) the trapped electrons possess a broad energy spectrum (about 100% spread) with maxima at 0.5 GeV (for $\gamma_{e0} = 125$) or 0.75 GeV (for $\gamma_{e0} = 42$) and a cutoff at $\approx$1 GeV. Tuning the energy of injected electrons to the resonance with a given wake period reduces the final root-mean-square (rms) emittance of the accelerated electron bunch but has no effect on the final energy spread.

Acceleration of electron bunches injected with energies far below resonant is discussed in Sec. V. Simulations show that electrons with initial energies of 5 and 1 MeV not only are effectively trapped and accelerated up to 1 GeV, but also have substantially less energy spread and lower rms emittance than those in the resonant case discussed in Sec. IV. Slow electrons ($\gamma_{e0} = 0.08\gamma_g$ and $\gamma_{e0} = 0.016\gamma_g$) loaded near the bottom of the 2D potential well slip into the accelerating and focusing phase and get as effectively accelerated as the electrons initially loaded in that phase. In particular, acceleration of 1 MeV electrons over twice the Rayleigh length produces a group of electrons with energy 900 ± 50 MeV and rms emittance less than 10^{-4} mm mrad.

Summary of the results and conclusions are offered in Sec. VI. In Appendix A, an analytical treatment is given for those nonlinear phenomena which have an effect on the propagation of ultrashort laser pulses in plasmas. The features of the plasma wakefield generated by diffracting Gaussian short laser beam are considered in Appendix B.

II. SHORT LASER PULSE PROPAGATION IN TENUOUS PLASMA: COMPENSATION OF RELATIVISTIC AND PONDEROMOTIVE NONLINEARITIES

Relativistic and ponderomotive nonlinearities for a short ($\omega_p \tau_L < 1$) and broad ($k_p r_0 > 1$), overcritical ($P > P_{\rm cr}$) laser pulse partly cancel each other.[9] The vacuumlike propagation of such pulses,[10] however, is not immune to the residual effect of the noncompensated relativistic nonlinearity (see Appendix A). We simulate the laser propagation, plasma wakefield excitation, and acceleration of injected test electrons by means of the 2D axially symmetric, fully relativistic, time-averaged particle code WAKE,[5,6] which is based on quasistatic[9] and extended paraxial[11] approximations. The normalized, slowly varying amplitude (envelope) of the laser vector potential $a(\xi, r, z)$ is evaluated as a function of the radial r and longitudinal z space variables and the retarded time $\xi/c = t - z/c$. In the simulations, the pulse propagates from left to right through a plasma slab centered at the vacuum focal plane $z = 0$. Simulation starts at a plane $z = z_0 < 0$ and terminates at the symmetric plane $z = |z_0|$. Incident laser beam is described by the parameters listed in the Introduction, and has a Gaussian temporal and radial profile described by[12]

$$a = a_0(r, \xi, \zeta_0)\exp[-2\ln 2(\xi - \xi_0)^2/(c\tau_L)^2 + i\Psi_0], \qquad (1)$$

where $\zeta_0 = -z_0/Z_R$, $\Psi_0 = (r/r_0)^2\zeta_0/(1+\zeta_0^2) - \arctan\zeta_0$; $a_0(r, \zeta_0) = a_0(1+\zeta_0^2)^{-1/2}\exp[-(r/r_0)^2/(1+\zeta_0^2)]$; $\xi = \xi_0$ corresponds to the pulse center; and τ_L is the pulse full width at half maximum (FWHM) in intensity. At the starting point, the laser pulse (1) is given a converging (concave) phase front and focuses into plasma. The simulation proceeds from $z = -Z_R$ to $z = Z_R$, where $Z_R \approx 4$ cm for the parameters chosen.

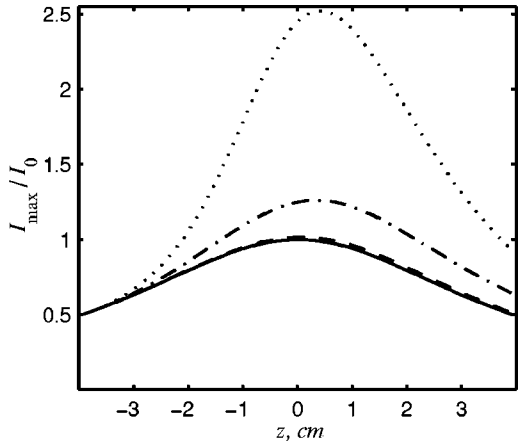

FIG. 1. The maximum intensity of a laser pulse on-axis as a function of propagation distance. The vacuum focal plane is $z=0$. The intensity is normalized to the maximum intensity of laser pulse in the focal plane in vacuum, $I_0=6.4\times10^{18}$ W/cm^2. Solid line corresponds to focusing in vacuum; other lines correspond to focusing into plasmas: dashed line—$n_0/n_c=1.6\times10^{-5}$ ($P=P_{cr}$), dash-dotted line—$n_0/n_c=6.4\times10^{-5}$ ($P=4P_{cr}$), dotted line—$n_0/n_c=1.28\times10^{-4}$ ($P=8P_{cr}$), where $n_c=1.75\times10^{21}$ cm^{-3} is the critical density.

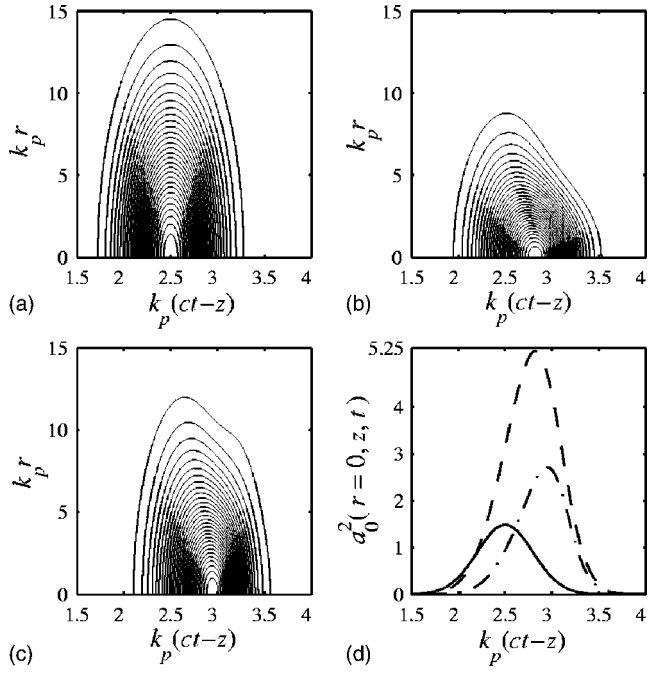

FIG. 2. Contour plots of the normalized pulse intensity at three positions: (a) $z=-Z_R$, (b) $z=0$, (c) $z=Z_R$. At $z=-Z_R$ the pulse is Gaussian (1). Its amplitude $a_0=1.72$, radius $k_p r_0=7.84$, and duration $\omega_p\tau_L=0.68$ provide $P\approx6P_{cr}$. The solid, dashed, and dotted-dashed lines in the plot (d) show the on-axis profile of intensity for the plots (a), (b), and (c).

The normalized amplitude of the laser at the vacuum focus is $a_0=1.72$.

A set of simulations with different plasma densities demonstrates the effect of nonlinearities on the pulse evolution. The maximum laser intensity on axis ($r=0$) is plotted in Fig. 1 versus propagation distance. The density $n_0=n_{SF}=2.8\times10^{16}$ cm^{-3} corresponds to $P=P_{cr}$ (dashed line). At $n_0=8n_{SF}$ (or $P=8P_{cr}$, dotted line), the noncompensated relativistic self-focusing leads to an intensity increase of a factor of 2.5 in the vicinity of the focal plane. For $n_0=4n_{SF}$ (or $P=4P_{cr}$), the on-axis variation of laser intensity is still very close to that in the vacuum case (dash-dotted line in Fig. 1). Therefore, under appropriate choice of parameters and contrary to the case of longer laser pulses,[7] propagation of a relativistically strong, formally overcritical ultrashort pulse is not challenged by relativistic self-focusing in a rarefied plasma.

Figure 2 demonstrates the distortion of the laser radial and temporal profiles due to the uncompensation of relativistic self-focusing. For $P\approx6P_{cr}$, the contour plots of normalized intensity $a^2(\xi,r)$ show that leading part of the pulse spreads in the course of propagation while the trailing part shrinks. The effect manifests in full in the vicinity of the vacuum focal plane. The difference between the speed of light in vacuum and the pulse group velocity in plasma brings about a gradually growing shift of the pulse center from its initial position in the comoving frame.

The analytical treatment given in Appendix A of a weakly relativistic approximation predicts an amplitude threshold a_{0c} [see Eq. (A11)], below which the laser pulse radially spreads according to the linear theory of diffraction for Gaussian beams.[12] For a Gaussian temporal profile, the critical amplitude is $a_{0c}=(\omega_p\tau_L)^{-1}\sqrt{4\ln2/[1+(k_p r_0/4)^2]}$. In Fig. 2, the laser amplitude $a_0=1.72$ used in the simulation of exceeds the critical amplitude $a_{0c}\approx1.11$, which explains the pronounced manifestation of the nonlinearity. In order to find out how to reduce the adverse effect of uncompensated nonlinearities, we simulate the wakefield evolution and electron acceleration in plasmas of lower density. In particular, we chose the case $P=4P_{cr}$ (i.e., a plasma density of $n_0=1.12\times10^{17}$ cm^{-3} giving $a_{0c}\approx1.6$). The relativistic factor of the laser pulse is then $\gamma_g=125$ and the normalized pulse duration is $\omega_p\tau_L\approx0.56$.

III. EXCITATION OF NONLINEAR PLASMA WAKEFIELD BY SHORT DIFFRACTING NEARLY GAUSSIAN LASER PULSE

We study numerically and analytically the plasma wakefield evolution in a regime where the laser nonlinearities are mostly compensated and the laser beam is close to Gaussian; the parameters are taken as suggested at the end of Sec. II. The intensity on axis is high enough to produce an electron density perturbation of the order of the background plasma density. The wake becomes strongly nonlinear in the vicinity of the focal plane, $z=0$, where its amplitude reaches the maximum. The radial and temporal profiles of the laser pulse and electron density distribution for this plane are shown in Fig. 3. The wakefield is far from harmonic: the regions of density depression are much broader than the crests. Moreover, the wake phase front is not planar and its curvature builds up with time. The relativistic shift of plasma frequency in the wake is proportional, to the lowest order, to the laser intensity squared, which varies radially and thus brings about the said curvature.[13] The radial phase variation, however, does not produce a radial wave breaking[14] for at least six wake periods.

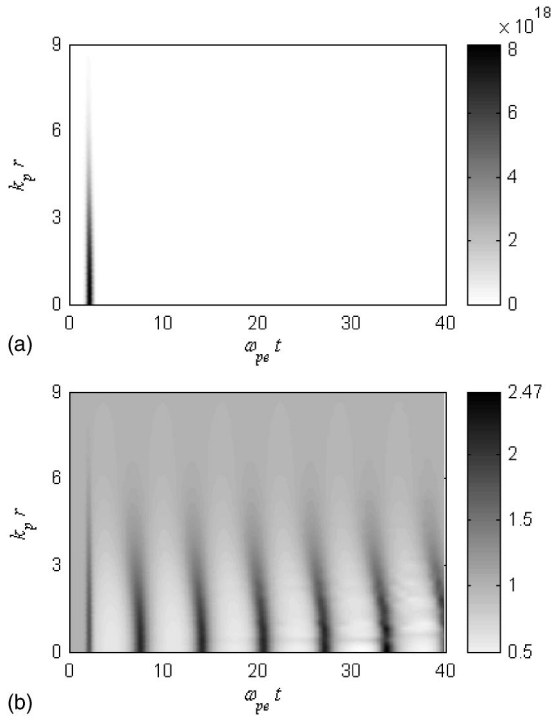

FIG. 3. Temporal evolution of (a) the radial profile of laser pulse intensity (in W/cm^2) and (b) the electron density normalized to the background density n_0 at the plane $z=0$ (vacuum focus).

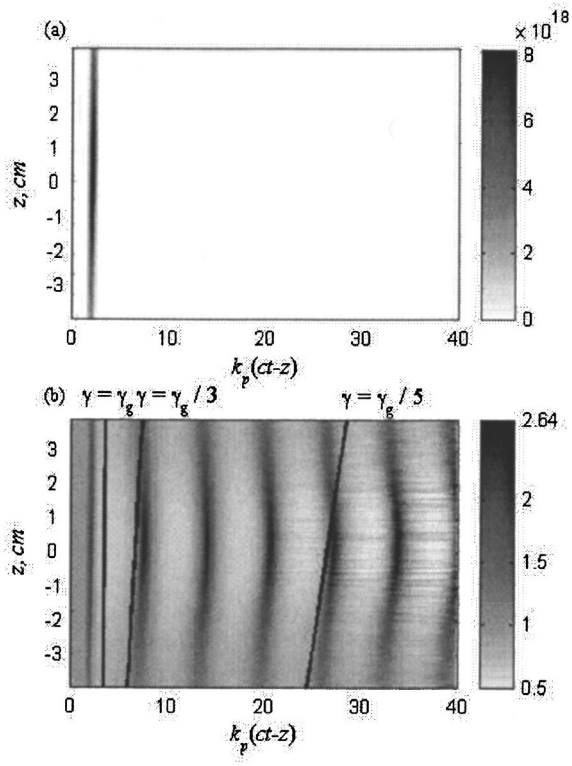

FIG. 4. On-axis evolution of (a) the laser intensity (in W/cm^2) and (b) the electron density normalized to the background density n_0 as a function of retarded time and laser pulse propagation length in the simulation of Fig. 3. The solid lines in the plot (b) are the tangents to the electron density crests. They characterize the local phase velocity of the wake at $z=z_0=-Z_R$. Corresponding relativistic factors in units of $\gamma_g=125$ are shown at the top line of the plot (b).

The wake phase velocity is not constant along the laser path. This effect has a purely relativistic origin. As the pulse focuses at $z<0$, its intensity grows, and so does the relativistic shift of plasma frequency. The wake period stretches and the phase velocity drops below the group velocity of laser. Beyond the focal plane, $z>0$, the pulse radially spreads and the plasma period gradually shrinks thus tending back to the linear limit τ_p. At this stage, the wake phase velocity may exceed both laser pulse group velocity in plasma and the speed of light in vacuum. It is known that the wake phase can reach the vacuum speed of light at some point along the laser pulse path in a longitudinally inhomogeneous plasma.[8] In the regime we consider, this occurs in the *uniform* plasma due to the nonlinear frequency variation of the plasma wake driven by the diffracting laser. Figure 4 shows the on-axis laser intensity (a) and the electron density (b) versus retarded time and distance z in plasma. The plot (b) demonstrates the phase "deceleration" ("acceleration") at $z<0$ ($z>0$) with the wake period stretching (contracting). At $z>0$ the wake phase velocity is clearly superluminous.

An electron falls in resonance with the accelerating wakefield if its velocity v_{e0} coincides at the point of injection with the local phase velocity of wake. Taking tangents to the electron density crests in Fig. 4(b) allows us to evaluate the resonant Lorentz factor $\gamma_{e0}\gg 1$ of the electron injected on axis at $z_0=-4$ cm. The tangent equation, $z\approx 2\xi\gamma_{e0}^2$, gives $\gamma_{e0}\approx 42\approx\gamma_g/3$ for the second and $\gamma_{e0}\approx 21=\gamma_g/5$ for the fifth wake period. In weakly nonlinear theory of wakefield excitation by a diffracting short Gaussian laser pulse (see Appendix B), the wake Lorentz factor is expressed as a function of normalized pulse position $\zeta=z/Z_R$ and time delay ξ/c [see Eq. (B5)], yielding estimates of γ_{e0} which are a factor of 2 higher than those inferred from the graphical estimates of Fig. 4(b).

IV. ACCELERATION OF RESONANT ELECTRON BUNCHES

The test electron bunch is injected in the laser wake at $z_0=-Z_R$. At this point, a Monte-Carlo generator creates monoenergetic particles with energy $mc^2\gamma_{0e}$ and uniform distribution over a time interval τ_b. The bunch has a transverse momentum spread, which results in a nonzero initial angular divergence $\langle\alpha^2\rangle^{1/2}=\alpha_e$ and a nonzero initial rms emittance $\varepsilon_\perp=(1/2)[\langle r_\perp^2\rangle\langle(p_\perp/p)^2\rangle-\langle(\mathbf{r}_\perp\cdot\mathbf{p}_\perp)/p\rangle^2]^{1/2}$ (Ref. 15). Initially, the radial distribution of electron density in the bunch is Gaussian with a rms radius $\sigma\sim r_0$. The accelerated electrons are extracted from the wake at $z=Z_R$.

First, the conventional resonant condition $\gamma_{e0}=\gamma_g$ is considered. A bunch of 5000 test electrons with $\gamma_{e0}=125$, zero angular divergence, and $k_p\sigma=k_p r_0/\sqrt{2}=4.5$ is accelerated in the second wake period ($6.5\leqslant k_p\xi\leqslant 13$, which corresponds to a bunch duration of $\tau_b\approx 330$ fs). Distributions of test electrons in coordinate and momentum space at $z=Z_R$, and final energy versus injection phase are shown in Fig. 5. The gray-scale background in the plot (a) is the normalized potential $\langle\psi\rangle=[e/(mc^2)]\langle A_z-\Phi\rangle$, where $\langle\cdots\rangle$ means averaging over the laser period $2\pi/\omega_0$, and $\langle A_z\rangle$ and $\langle\Phi\rangle$ are vector and scalar

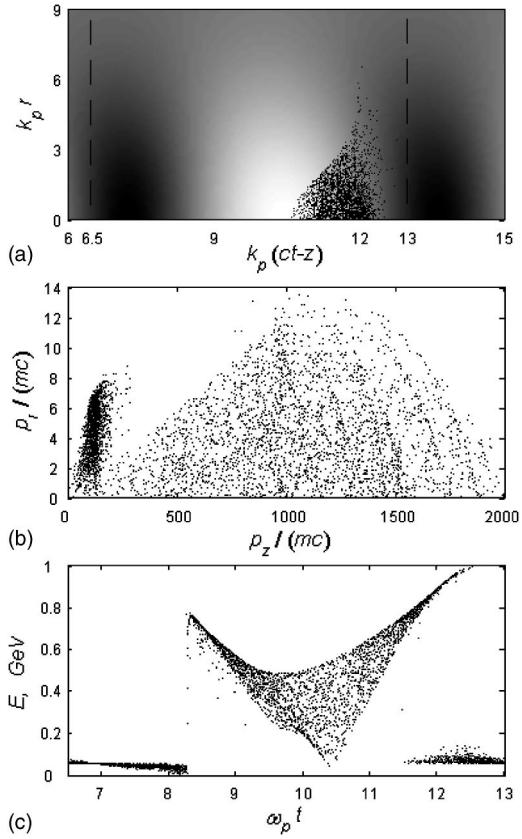

FIG. 5. Acceleration of the resonant electron bunch ($\gamma_{e0}=\gamma_g=125$): (a) distribution in space, (b) momentum distribution, and (c) energy versus injection phase for test electrons crossing the extraction plane, $z=Z_R$. Each dot corresponds to a numerical electron. The density of dots provides the number of test particles per elementary volume $k_p^2 dr\, d\xi$ in the coordinate space in the plot (a) and per elementary volume $(dp_r dp_z)/(mc)^2$ in the momentum space in the plot (b). The grayscale density in the plot (a) is proportional to the normalized wakefield potential $\langle\psi\rangle$, the lightest gray corresponds to $\langle\psi\rangle_{\max}=0.3$, the darkest gray corresponds to $\langle\psi\rangle_{\min}=-0.24$. Dashed lines in the plot (a) show the boundaries of the bunch at the injection plane, $z=-Z_R$.

potentials associated with the low-frequency wakefields. These potentials determine the low-frequency electric and magnetic fields in plasma, and, hence, the forces acting on the test electrons.[6] The plot (a) shows that the accelerated particles are collected in the focusing and accelerating quarter of the wakefield period. Quite a few electrons stay near the bottom of the potential well with an almost negligible energy gain, as testified by the plot (c). The transverse spread of the bunch is reduced by roughly a factor of 2 compared with the initial value.

Figure 6 shows the final energy and emittance of the test electrons collected by equally distributed channels of an electron spectrometer. We compare them for the two different resonant conditions which could be fulfilled at the injection plane. The thick lines correspond to $\gamma_{e0}=\gamma_g=125$ (resonance with the laser pulse) and the thin ones to $\gamma_{e0}=\gamma_{p0}\approx 42$ (resonance with the second wake period on axis). In both cases, the energy spectrum is described by a shelf with a not-too-pronounced maximum near 0.5 GeV for $\gamma_{e0}=125$ and 0.75 GeV for $\gamma_{e0}=42$. There is no energy gap between the accelerated particles and the bulk of electrons. In the case

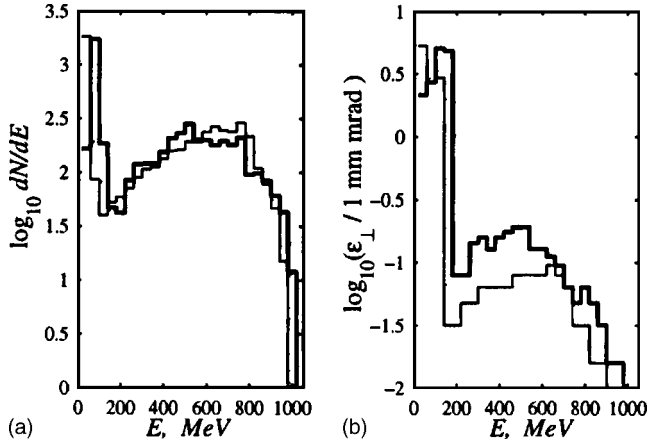

FIG. 6. Energy spectrum (a) and emittance (b) at the extraction plane, $z=Z_R$, for electron bunches injected with $\gamma_{e0}=125$ (thick lines) and $\gamma_{e0}=42$ (thin lines) into the second wake period.

of $\gamma_{e0}=42$ the final emittance is smaller than that for $\gamma_{e0}=125$ [see the plot (b)]. The energy cutoff appears to be independent of the injected electron energy and is close to 1 GeV.

The energy limit of 1 GeV can be exceeded if the electrons are injected earlier and extracted from the wake later. Additional runs show that elongating the acceleration length by 50% ($-1.5Z_R\leqslant z\leqslant 1.5Z_R$) gives a 15% increase in the maximum final energy. As the highest acceleration gradients are achieved near the laser focus, increasing the acceleration length beyond $2Z_R$ does not lead to a substantial growth of electron energy.

Analysis of Figs. 5 and 6 leads to the following conclusion: injection of a long (of the order of or longer than a wake period) resonant electron bunch results in a large energy spread of trapped and accelerated electrons no matter whether the injected bunch was resonant with the laser pulse or with a given period of the wake. The simulations show that the resonant conditions $\gamma_{e0}=\gamma_g$ or $\gamma_{e0}=\gamma_{p0}$ only minimize energy spread for the electrons injected in just one quarter (focusing and accelerating) of the wake period. A sample simulation made for a short electron bunch ($11.5\leqslant k_p\xi\leqslant 12.5$) with $\gamma_{e0}=125$ and zero initial emittance results in a mean output 0.85 GeV per electron with about 30% energy spread.

V. ACCELERATION OF NONRESONANT ELECTRON BUNCHES

In simulations with nonresonant electron bunches, the initial electron energies are substantially smaller than these in the resonant cases. Figure 7 presents the same plots as Fig. 5 but for injected electrons with $\gamma_{e0}=10\ll\gamma_{g(p0)}$.

Comparison of Figs. 5 and 7 reveals certain benefits of using nonresonant electrons for injection. First, the accelerated bunch of initially nonresonant particles is more compact in the radial direction [compare plots (a) of the two figures] and the radial momentum spread is lower [compare plots (b)]. Second, Fig. 7(a) shows that no electrons remain at the bottom of the potential well, $k_p\xi\approx 10$, indicating that all the trapped nonresonant electrons are accelerated, and an energy

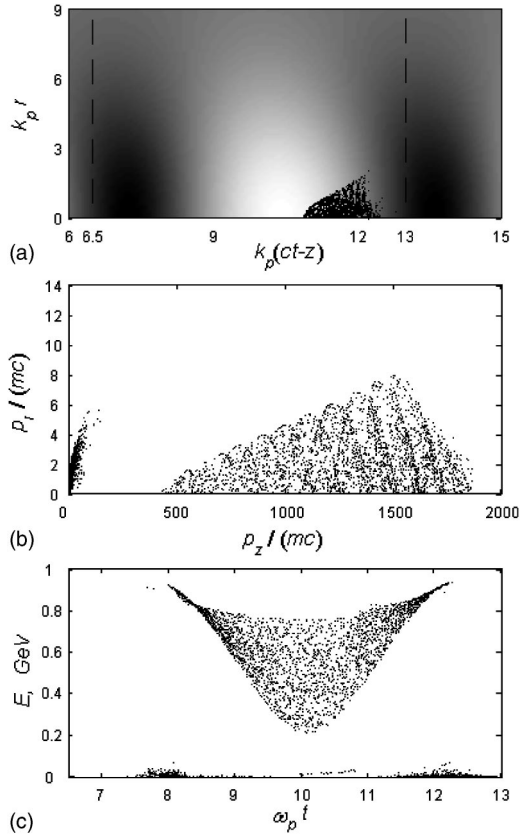

FIG. 7. Acceleration of the nonresonant electron bunch. All parameters being the same as in Fig. 5, except of initial relativistic factor of electrons $\gamma_{e0}=10\ll\gamma_g$.

gap appears between the trapped and nontrapped particles [see Fig. 7(c)]. Finally, in contrast to the resonant case, the nonresonant electrons gain almost the same amount of energy regardless whether they are loaded into the accelerating or decelerating focusing phases. At the point of injection, the wake phase outruns the nonresonant particles, so they slip out of the disadvantageous phase towards the focusing and accelerating one. Resonant electrons are initially at rest in the decelerating phase, so their slippage takes more time, and their final energy is consequently lower. By comparison with the resonant case [Fig. 8(b) versus 6(b)], the final emittance of the nonresonant bunch is typically significantly lower (by a factor of 3 for the spectrometer bins beyond 500 MeV).

The properties of the accelerated electrons also depend sensitively on which cycle of the wake is used to accelerate them. Figure 8 shows the final energy spectrum and emittance of initially nonresonant test electrons with $\gamma_{e0}=10$, injected at $z_0=-Z_R$ with zero initial emittance in the second ($6.5\leqslant k_p\xi\leqslant 13$, simulation of Fig. 7) and sixth ($32.1\leqslant k_p\xi\leqslant 38.4$) wake periods. The initial rms radius of the bunch is the same as in Figs. 5 and 7. The efficiency of acceleration clearly reduces when the time delay between the laser pulse and electron bunch grows. The spectrum of electrons accelerated in the second period has the maximum at 0.8 GeV and a sharp cutoff at 0.95 GeV. The accelerated electrons are separated from the bulk of low energetic particles by a gap of 150 MeV [see also Fig. 7(c)]. By contrast, acceleration in the sixth period gives a plateaulike energy spectrum which rises

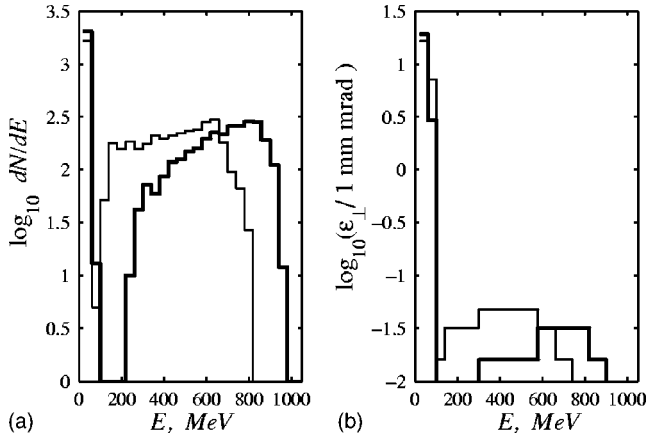

FIG. 8. Final (a) energy spectrum and (b) emittance of electrons injected in different wake periods. Electrons are injected with $\gamma_{e0}=10$. Thick and thin lines correspond to injection into the second (data from simulation of Fig. 7) and the sixth period, respectively.

steadily up to 0.65 GeV and drops at 0.85 GeV. Therefore, the injection time lag should be taken as small as possible in order to reduce the adverse effect of the wake phase velocity variation.

Technological limitations in monoenergetic electron injectors lead inevitably to use of long ($\tau_b\gg\tau_p$) and wide ($k_p\sigma\gg 2\pi$) electron bunches with nonzero rms emittance. The results of sample modeling of this situation are presented in Fig. 9. The energy spectrum (a) and rms emittance (b) of accelerated electrons are shown at the extraction point $z=Z_R$. The nonresonant ($\gamma_{e0}=10$) electron beam injected at $z_0=-Z_R$ covers three consecutive wake periods, $6.5\leqslant k_p\xi\leqslant 25.4$. The transverse size of the beam ($k_p\sigma=13.5$) is a factor of 3 larger than that of Figs. 5 and 7, and the number of particles in the bunch is 20 000. The thick lines correspond to the bunch with zero rms emittance at injection, and the thin lines to the case with initial rms emittance $\varepsilon_\perp=2.145$ mm mrad. Variation of the initial rms emittance has a negligible effect on the energy spectrum, which has a sharp maximum at 0.75 GeV and cutoff at 0.95 GeV. The presence

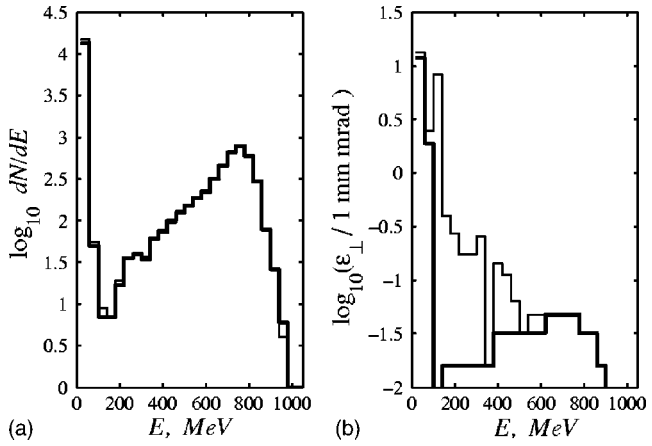

FIG. 9. Energy spectrum (a) and emittance (b) of accelerated electrons for nonresonant ($\gamma_{e0}=10$) wide ($k_p\sigma=13.5$) and long ($6.5\leqslant k_p\xi\leqslant 25.4$) electron bunch with the initial emittance of zero (thick lines) and 2.145 mm mrad (thin lines).

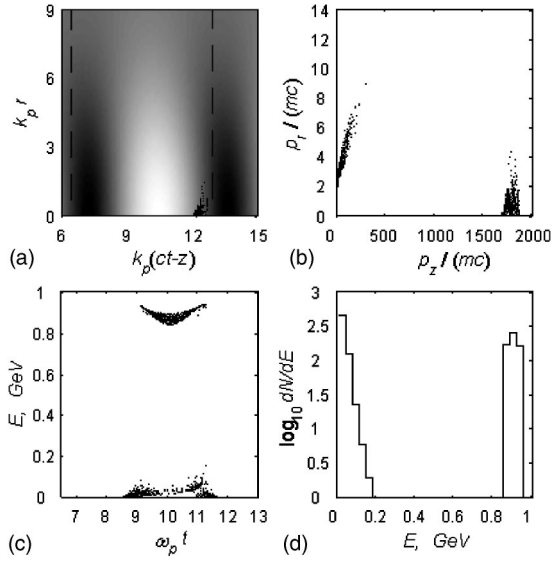

FIG. 10. Acceleration of a low-energy electron bunch ($\gamma_{e0}=2$). Plots (a)–(c) show the same quantities as in Figs. 5 and 7. The electron energy spectrum is shown in plot (d). Injection of highly nonresonant bunch provides almost monoenergetic acceleration of trapped electrons.

of a nonzero rms emittance in the injection beam increases the emittance of the low-energy electrons only (spectrometer bins at $E<500$ MeV). The emittance of higher-energy electrons is unaffected. Thus, these simulations show that elongating the electron bunch still preserves all the benefits of using nonresonant electrons, but is not challenging to implement experimentally.

Effective trapping and acceleration of electrons also occur for bunches injected with very low energy (about 1 MeV), leading to almost monoenergetic acceleration.[16] In Fig. 10, the energy spectrum is shown of accelerated electrons with initial relativistic factor $\gamma_{e0}=2$ and radial spread $k_p\sigma=2$, and the other parameters taken the same as in Figs. 5 and 7. The total number of injected particles is 2500, of which roughly one half is trapped and accelerated up to 900 MeV with 10% energy spread. The final rms emittance of accelerated bunch is lower than 10^{-4} mm mrad.

VI. CONCLUSION

Construction of petawatt ultrashort pulse lasers creates the opportunity to accelerate electrons to GeV energies by using the standard LWFA scheme. In quite tenuous plasmas ($\omega_p<\tau_L^{-1}$), the relativistic and ponderomotive nonlinearities of a not-very-tightly focused ($k_p r_0 \geqslant 2\pi$) laser pulse can cancel each other.[9] In this regime, an overcritical laser pulse propagates as if in vacuum. Increasing the laser focal spot up to 100 μm in radius elongates the laser-plasma interaction length (estimated as twice the Rayleigh length) up to 8 cm without any external optical guiding. Such loosely focused laser pulses, however, have enough energy to drive a nonlinear plasma wakefield throughout this distance, providing controlled acceleration of externally injected electrons up to 1 GeV. The nonlinear features of a quasi-plane-wave plasma wake facilitate trapping, focusing, and acceleration of the electrons from the injected bunch. The converging laser pulse drives a plasma wake whose period stretches (due to the relativistic decrease in plasma frequency) as the pulse approaches the focal plane. At this stage, the wake phase velocity drops below the pulse group velocity. Growth of the the wake amplitude combined with the decrease in the phase velocity provides the efficient trapping of low-energy (nonresonant) electrons. Beyond the focal plane, the laser pulse diverges, and the wake phase may become superluminous, which provides additional longitudinal compression of the electron bunch in the focusing and accelerating quarter of the wakefield period. These features of the wakefield structure reduce the energy spread and emittance of the electron bunch injected out of resonance with the wake, $\gamma_{e0} \ll \gamma_{g(p0)}$, and, in the limit of very low initial energy (about 1 MeV), provide almost monoenergetic acceleration. Therefore, the scheme considered here can be used as a part of a multistage high-energy electron accelerator.

The possibility of achieving the GeV-range electron energies has been considered so far only in plasma-channel guided LWFA in both weakly[17] and strongly[18] nonlinear regimes with a laser energy of a few joules. One joule is the energy of about 6×10^9 GeV electrons. Therefore, we can expect that the number of electrons in the GeV energy range accelerated by a few-joule laser will be far below 6×10^9, which is not suitable for staged acceleration. On the other hand, increasing the laser energy to 30 J in a channel-guided LWFA with the focal spot in the range between 7.4 μm (Ref. 18) and 70 μm (Ref. 17) leads to such strong plasma density perturbations that the controlled electron acceleration can hardly be expected. However, by employing loosely focused pulses with petawatt powers (or several tens of joules) we can avoid both these issues and produce well-controlled, monoenergetic, low-emittance GeV electron bunches with sufficient charge to be practical for multistaging to high final energies.

ACKNOWLEDGMENTS

The authors highly appreciate the assistance of N. Matlis in the preparation of the manuscript.

L.M.G. and S.Yu.K. gratefully acknowledge the hospitality of CPhT, École Polytechnique. This work was partly supported by Centre National de la Recherche Scientifique (France) in the frame of cooperation with the Russian Academy of Sciences, the École Polytechnique (in the form of postdoctoral fellowship for S.Yu.K.), the Russian Fund for Basic Research (Grant No. 02-02-1611), and the U.S. Department of Energy under Contracts No. DE-FG02-04ER54763 and No. DE-FG02-04ER41321.

APPENDIX A: NONLINEAR EFFECTS IN PROPAGATION OF ULTRASHORT LASER PULSES

Self-consistent evolution of axisymmetric laser pulse and perturbations of electron plasma density can be described in the weakly nonlinear quasistatic approximation by the set of equations[19]

$$2ik_0\frac{\partial a}{\partial z}+\Delta_\perp a=k_p^2\left(N-\frac{1}{4}|a|^2\right)a, \tag{A1a}$$

$$\frac{\partial^2 N}{\partial \xi^2} + k_p^2 N = \frac{1}{4}\left(\frac{\partial^2}{\partial \xi^2} + \Delta_\perp\right)|a|^2, \tag{A1b}$$

where $a = eE/(m\omega_0 c)$ is the normalized amplitude of the laser electric field, $N \equiv (n_e - n_0)/n_0$ is the normalized electron density perturbation, and $\Delta_\perp \equiv r^{-1}\partial/\partial r(r\partial/\partial r)$ is the radial part of the Laplace operator.

In the limit of a short and wide pulse whose length $c\tau_L$ is smaller but the radius r_0 is larger than k_p^{-1}, the main terms in Eq. (A1b) are those containing the second derivatives with respect to ξ. In this approximation, the nonlinear terms in the right-hand side (RHS) of Eq. (A1a) cancel each other, and the pulse propagates as in vacuum.[9] The small corrections to the index of refraction which are due to the finite pulse length and proportional to $(\omega_p \tau_L)^2$ were considered in Ref. 9. We consider the effect of small longitudinal and transverse nonlinearities on the evolution of a short laser pulse and assume the transverse pulse shape be Gaussian in every cross section,

$$a = \frac{A_0(\xi)}{f(\xi,z)} \exp\left[-\frac{r^2}{r_0^2 f^2} + i\left(\frac{r^2}{2}\beta(\xi,z) + \varphi(\xi,z)\right)\right]. \tag{A2}$$

Here, $f(\xi,z)$ is the dimensionless focal spot size (pulse width) which equals unity in the focal plane $z=0$ [i.e., $f(\xi,0)\equiv 1$]. The function $A_0(\xi)$ gives an initial amplitude profile on axis, the initial focal spot radius is r_0, the quantities $\varphi(\xi,z)$ and $\beta(\xi,z)$ give the on-axis values of phase and curvature of the laser phase front, respectively. Substituting Eq. (A2) into Eqs. (A1) gives the equation for the pulse width[20]

$$\frac{\partial^2 f}{\partial z^2} - \frac{f^{-3}}{Z_R^2} = -\frac{f}{4}\frac{\omega_p k_p^3}{\omega_0 Z_R}\int_{-\infty}^{\xi} d\xi' \sin[k_p(\xi-\xi')]\frac{A_0^2(\xi')}{f^4(\xi',z)} \times\left(1 + \frac{16}{k_p^2 r_0^2 f^2(\xi',z)}\right), \tag{A3}$$

where z is the coordinate of the pulse center moving from the left to the right; the transverse Laplace operator in Eq. (A1b) gives the second term in the brackets in the integrand. In the short-pulse case, $A_0^2(\xi)$ is nonzero within an interval $|\xi| \ll k_p^{-1}$. Integrating by parts the expression in the RHS of Eq. (A3) and taking account of only the main term gives

$$\frac{\partial^2 f}{\partial z^2} - \frac{f^{-3}}{Z_R^2} = -\frac{f}{4}\frac{\omega_p k_p^3}{\omega_0 Z_R}\int_{-\infty}^{\xi} d\xi' \int_{-\infty}^{\xi'} d\xi'' \frac{A_0^2(\xi'')}{f^4(\xi'',z)} \times\left(1 + \frac{16}{k_p^2 r_0^2 f^2(\xi'',z)}\right). \tag{A4}$$

The laser pulse of small amplitude propagates in plasma as in vacuum. In order to evaluate the threshold amplitude a_{0c} above which the effect of nonlinearities might occur, we consider Eq. (A4) near the focal plane, $z=0$. The pulse width f is constant there, while $A_0(\xi)$ alters within a relatively short interval $|\xi| \ll k_p^{-1}$. We assume that $f(\xi,z)$ varies with ξ slower than $A_0(\xi)$ within some segment of the laser path. Equation (A4) then reduces to

$$\frac{\partial^2 f}{\partial \zeta^2} - \frac{1}{f^3}\left\{1 - \alpha I(\xi)\left(1 + \frac{2}{\alpha f^2}\right)\right\} = 0, \tag{A5}$$

where $\zeta = z/Z_R$ is the normalized propagation distance, $\alpha = (k_p r_0)^2/8$ is the normalized initial squared spot size, and

$$I(\xi) = k_p^2 \int_{-\infty}^{\xi} d\xi' \int_{-\infty}^{\xi'} d\xi'' A_0^2(\xi''). \tag{A6}$$

The condition $f(\xi,0)\equiv 1$ gives the integral of Eq. (A5),

$$\left(\frac{\partial f}{\partial \zeta}\right)^2 - \left(1 - \frac{1}{f^2}\right)\left[1 - \alpha I - I\left(1 + \frac{1}{f^2}\right)\right] = 0. \tag{A7}$$

Initially, the evolution of a small spot size perturbation $\delta f = f - 1$, $|\delta f| < 1$, obey the equation following from Eq. (A7),

$$(\partial \delta f/\partial q)^2 - 2\delta f(B-1) = 0, \tag{A8}$$

where $q = \zeta\sqrt{I}$, and $B = I^{-1} - 1 - \alpha$. Equation (A8) has real solutions for both $B<1$ (then $\delta f<0$) and $B>1$ (then $\delta f>0$). Reduction of the pulse width in the first case corresponds to the converging laser pulse, while in the second case the laser diverges. The border of laser pulse stability against the transverse distortions, $B=1$, gives the implicit equation for the stability point,

$$I(\xi_c) = (2+\alpha)^{-1}. \tag{A9}$$

The point ξ_c separates diverging and converging parts in the pulse profile. The function $I(\xi)$ grows monotonically from the leading front towards the trailing edge of the pulse. Therefore, the pulse portion which lays between the leading front and the point ξ_c spreads, while the part beyond ξ_c focuses. As a result, in the course of propagation the pulse acquires the "beet-root" shape. In the vicinity of the threshold point ξ_c, the pulse width given by Eq. (A8) reads $f = 1 - (\zeta^2/2)[I(\xi) - I(\xi_c)]/I(\xi_c)$.

We examine the case of a Gaussian laser pulse, $A_0(\xi) = a_0 \exp[-2\ln 2\,\xi^2/(c\tau_L)^2]$, with the center located at $\xi=0$. Substituting $A_0(\xi)$ into Eq. (A6) gives

$$I(\xi) = \frac{(a_0\omega_p\tau_L)^2}{8\ln 2}\int_{-2\sqrt{\ln 2}\,\xi/(c\tau_L)}^{\infty} dx[1 - \Phi(x)], \tag{A10}$$

where

$$\Phi(x) = \frac{2}{\sqrt{\pi}}\int_0^x dt \exp(-t^2)$$

is the probability integral. Substantial modification of the laser pulse shape occurs when the threshold condition (A10) is met at the pulse center (i.e., $\xi_c = 0$). In consistence with Eq. (A10), this criterion takes the form

$$a_{0c} = \frac{1}{\omega_p \tau_L}\sqrt{\frac{4\ln 2}{1+(k_p r_0/4)^2}}. \tag{A11}$$

APPENDIX B: THE WAKEFIELD OF AN ULTRASHORT FOCUSING LASER PULSE

The wakefield is excited by the ponderomotive force associated with a laser pulse. Under the assumption that the linear theory of diffraction of Gaussian beams[12] holds, the laser pulse envelope $a(r,z,\xi)$ reads

$$a = \frac{a_0}{\sqrt{1+\zeta^2}}\exp\left[-2\ln 2\frac{\xi^2}{(c\tau_L)^2} - \frac{r^2}{r_0^2(1+\zeta^2)} + i\Psi\right], \tag{B1}$$

where $\zeta = z/Z_R$, $\xi = v_g t - (z+z_0)$, $\Psi = (r/r_0)^2\zeta/(1+\zeta^2) - \arctan\zeta$, v_g is the group velocity of a pulse, other notations are the same as in Eq. (1). At $t=0$, the pulse center $\xi=0$ resides at $z=-z_0$. The pulse propagates towards positive z.

In the linear approximation, the frequency of an electron plasma oscillation equals ω_p and the phase velocity v_p of the wake coincides with the pulse group velocity v_g. In the weakly nonlinear approximation, the frequency of plasma oscillations is downshifted because of relativistic increase of the mass of oscillating electron.[21] Intensity of the Gaussian beam (B1) varies along the laser path and so does the amplitude of a plasma wake. Hence, relativistic reduction of the plasma frequency alters as a function of propagation distance, and this phase slippage characterizes the variation of the phase velocity. Consideration of this effect is easier in the case of a loosely focused, $k_p r_0 \gg 1$, and not so intense, $a_0 < 1$, laser pulse, when the wake electric field is the potential one. Then, for the laser pulse amplitude taken in the form (B1), the dimensionless wake potential $\phi = e\varphi/(mc^2)$ is given by[3]

$$\phi = -\frac{(a_0/2)^2 g(x)}{1+\zeta^2}\exp\left[-\frac{2r^2}{r_0^2(1+\zeta^2)}\right] \times \sin\left\{\left[k_p + \frac{\Delta\omega_p(z,r)}{c}\right]\xi\right\}, \tag{B2}$$

where $g(x) = x\sqrt{\pi/2}\exp(-x^2/8)$ depends on the dimensionless pulse length $x = \omega_p\tau_L/\sqrt{2\ln 2}$, the relativistic frequency shift[19] is $\Delta\omega_p = -(3/16)\omega_p[(a_0/2)^2/(1+\zeta^2)]^2\exp[-(2r/r_0)^2/(1+\zeta^2)]g^2(x)$. The on-axis phase of the wake potential follows from Eq. (B2):

$$\theta = k_p(v_g t - z)\left\{1 - \frac{3}{16}\left[\frac{(a_0/2)^2 g(x)}{1+\zeta^2}\right]^2\right\}. \tag{B3}$$

Then, the wake phase velocity v_p reads

$$v_p = -\frac{\partial\theta/\partial t}{\partial\theta/\partial z} \approx v_g\left\{1 + \frac{3}{4}\left[\frac{(a_0/2)^2 g(x)}{1+\zeta^2}\right]^2\frac{\zeta\xi/Z_R}{1+\zeta^2}\right\}. \tag{B4}$$

The quantity ξ/v_g characterizes a positive time delay with respect to the pulse center and ζ characterizes the laser pulse position relative to the focal plane. When the pulse passes the focal plane, ζ becomes positive. The wake phase velocity coincides with the pulse group velocity only far away from the focal plane and exactly at the focal plane. The wake phase velocity decreases while the pulse approaches the focal plane and reaches the minimum value for $z=-Z_R/\sqrt{5}$ where $v_p \approx v_g\{1-0.192[(a_0/2)^2 g(x)]^2\xi/Z_R\}$. The wake phase velocity exceeds v_g and can exceed the vacuum speed of light while the pulse moves away from the focal plane and radially spreads. The phase velocity variation can considerably modify the Lorentz factor $\gamma_{p0} \equiv (1-v_p^2/c^2)^{-1/2}$ if compared with $\gamma_g \equiv (1-v_g^2/c^2)^{-1/2}$ Eq. (B4) gives

$$\gamma_{p0}^{-2} \approx \gamma_g^{-2} + \frac{3}{2}\left[\frac{(a_0/2)^2 g(x)}{1+\zeta^2}\right]^2\frac{\zeta\xi/Z_R}{1+\zeta^2}. \tag{B5}$$

The electrons are injected at negative ζ where $v_p < v_g$. Hence, the resonance with the nonlinear wakefield needs less electron energy ($mc^2\gamma_{p0}$) than the resonance with the laser pulse (or a linear wakefield) $mc^2\gamma_g$.

Although Eq. (B5) is weakly relativistic, we use it to estimate resonant γ factors of different wake periods for the simulation parameters of Secs. IV and V ($\omega_p\tau_L = 0.56$, $a_0 = 1.72$, $k_p r_0 = 6.3$, $Z_R = 4$ cm, $\gamma_g = 125$). The accelerating phase of the second period (see Fig. 5) corresponds to $k_p\xi \approx 6.5$ (i.e., $\xi = -0.01$ cm), and, at the point of injection, $\zeta = -1$, the γ factor is $\gamma_{p0} \approx 80$. For the accelerating phase of the fifth wake period ($k_p\xi \approx 25$), Eq. (B5) gives $\gamma_{p0} \approx 49$. Graphic estimates of resonant Lorentz factors in Fig. 4(b) exceed the weakly relativistic estimates roughly by a factor of 2.

[1] T. Tajima and J. M. Dawson, Phys. Rev. Lett. **43**, 267 (1979).
[2] E. Esarey, P. Sprangle, J. Krall, and A. Ting, IEEE Trans. Plasma Sci. **PS-24**, 252 (1996).
[3] F. Amiranoff, S. Baton, D. Bernard *et al.*, Phys. Rev. Lett. **81**, 995 (1998); F. Dorchies, F. Amiranoff, V. Malka *et al.*, Phys. Plasmas **6**, 2903 (1999).
[4] M. Aoyama, K. Yamakawa, Y. Akahane, J. Ma, N. Inoue, H. Ueda, and H. Kiriyama, Opt. Lett. **28**, 1594 (2003).
[5] T. M. Antonsen, Jr. and P. Mora, Phys. Rev. Lett. **69**, 2204 (1992); Phys. Fluids B **5**, 1440 (1993).
[6] P. Mora and T. M. Antonsen, Jr., Phys. Rev. E **53**, R2068 (1996); Phys. Plasmas **4**, 217 (1997).
[7] A. G. Litvak, Sov. Phys. JETP **30**, 344 (1969); G.-Z. Sun, E. Ott, Y. C. Lee, and P. Guzdar, Phys. Fluids **30**, 526 (1987).
[8] T. Katsouleas, Phys. Rev. A **33**, 2056 (1986); P. Sprangle, B. Hafizi, J. R. Peñano, R. F. Hubbard, A. Ting, A. Zigler, and T. M. Antonsen, Jr., Phys. Rev. Lett. **85**, 5110 (2000); P. Sprangle, B. Hafizi, J. R. Peñano *et al.*, Phys. Rev. E **63**, 056405 (2001).
[9] P. Sprangle, E. Esarey, and A. Ting, Phys. Rev. Lett. **64**, 2011 (1990); Phys. Rev. A **41**, 4463 (1990).
[10] J. Faure, V. Malka, J.-R. Marquès, P.-G. David, F. Amiranoff, K. Ta Phuoc, and A. Rousse, Phys. Plasmas **9**, 756 (2002); C. Delfin, V. Lokhnygin, J. Mauritsson, A. Sjögren, C.-G. Wahlström, A. Pukhov, and G. D. Tsakiris, *ibid.* **9**, 937 (2002).
[11] J.-R. Marquès, F. Dorchies, F. Amiranoff *et al.*, Phys. Plasmas **5**, 1162 (1998).
[12] J. T. Verdeyen, *Laser Electronics* (Prentice-Hall, Englewood Cliffs, NJ, 1981), p. 53.
[13] C. D. Decker, W. B. Mori, and T. Katsouleas, Phys. Rev. E **50**, R3338 (1994); S. V. Bulanov, F. Pegoraro, and A. M. Pukhov, Phys. Rev. Lett. **74**, 710 (1995); N. E. Andreev, L. M. Gorbunov, and R. R. Ramazashvili, Plasma Phys. Rep. **23**, 277 (1997).
[14] S. V. Bulanov, F. Pegoraro, A. M. Pukhov, and A. S. Sakharov, Phys. Rev. Lett. **78**, 4205 (1997).
[15] P. Mora, J. Appl. Phys. **71**, 2087 (1992).
[16] R. F. Hubbard, D. F. Gordon, A. Ting *et al.*, Bull. Am. Phys. Soc. **48**, 106 (2003).
[17] P. Sprangle, J. R. Peñano, B. Hafizi *et al.*, Phys. Plasmas **9**, 2364 (2002).

[18]F. S. Tsung, R. Narang, W. B. Mori, C. Joshi, R. A. Fonseca, and L. O. Silva, Phys. Rev. Lett. **93**, 185002 (2004).
[19]N. E. Andreev, L. M. Gorbunov, V. I. Kirsanov, A. A. Pogosova, and R. R. Ramazashvili, JETP Lett. **55**, 571 (1992).
[20]N. E. Andreev, V. I. Kirsanov, and L. M. Gorbunov, Phys. Plasmas **2**, 2573 (1995).
[21]M. N. Rosenbluth and C. S. Liu, Phys. Rev. Lett. **29**, 701 (1972); C. J. McKinstrie and D. W. Forslund, Phys. Fluids **30**, 904 (1987).